RSC Advances

PAPER

View Article Online
View Journal | View Issue

Cite this: *RSC Adv.*, 2019, **9**, 21544

Effects of water, ammonia and formic acid on HO_2 + Cl reactions under atmospheric conditions: competition between a stepwise route and one elementary step†

Tianlei Zhang, *[ad] Yongqi Zhang,‡[ad] Mingjie Wen,‡[ad] Zhuo Tang,‡[a] Bo Long, *[b] Xiaohu Yu,[a] Caibin Zhao[a] and Wenliang Wang *[c]

Quantum chemical calculations at M06-2X and CCSD(T) levels of theory have been performed to investigate the effects of H_2O, NH_3, and HCOOH on the HO_2 + Cl → HCl + O_2 reaction. The results show that catalyzed reactions with three catalysts could proceed through two different mechanisms, namely a stepwise route and one elementary step, where the former reaction is more favorable than the latter. Meanwhile, for the stepwise route, a single hydrogen atom transfer pathway in the presence of all catalysts has more advantages than the respective double hydrogen atom transfer pathway. Then, the relative impacts of catalysts under tropospheric conditions were investigated by considering the temperature dependence of the rate constants and the altitude dependence of catalyst concentrations. The calculated results show that at 0 km altitude, the HO_2 + Cl → HCl + O_2 reaction with catalysts, such as H_2O, NH_3, or HCOOH, cannot compete with the reaction without a catalyst, as the effective rate constant with a catalyst is smaller by 2–6 orders of magnitude than the naked reaction within the temperature range 280–320 K. The calculated results also show that at altitudes of 5, 10 and 15 km, the effective rate constant of the HCOOH-catalyzed reaction increases obviously with an increase in altitude. At 15 km altitude, its value is up to 9.63×10^{-11} cm^3 per molecule per s, which is close to the corresponding value of the reaction without a catalyst, showing that the contribution of HCOOH to the HO_2 + Cl → HCl + O_2 reaction cannot be neglected at high altitudes. The new findings in this investigation are not only of great necessity and importance for elucidating the gas-phase reaction of HO_2 with Cl in the presence of acidic, neutral and basic catalysts, but are also of great interest for understanding the importance of other types of hydrogen abstraction in the atmosphere.

Received 11th May 2019
Accepted 27th June 2019

DOI: 10.1039/c9ra03541a

rsc.li/rsc-advances

1. Introduction

HO_2 is an important atmospheric species and plays important roles in both the troposphere and the stratosphere.[1] Meanwhile, HO_2 plays a significant transient intermediate role in the combustion of hydrocarbon fuels, atmospheric photolysis cycles, and biochemical processes.[2,3] The chlorine radical (Cl) plays an important role in the destruction of the stratospheric ozone layer. In the stratosphere, Cl is produced by the direct photolysis of dimers of the ClO_x family (ClO, ClO_2 *etc.*).[4,5] Also, Cl is mainly present in the form of reservoirs like HOCl, HCl, $ClONO_2$, *etc.* in the troposphere. These reservoirs are normally formed in the stratosphere and transported back to the troposphere. Consequently, due to the higher reactivity of Cl with the majority of organic compounds *etc.* as compared to OH radicals,[6,7] it is well known that Cl is a strong oxidant, and its reactions with atmospheric species, such as iodinated compounds and radicals, are expected to be important. Therefore, atmospheric sinks of Cl are of particular concern for fully elucidating atmospheric processes involving Cl.

Previous investigations have suggested that the gas-phase oxidation reaction of HO_2 by Cl (eqn (1)) is of interest in atmospheric chemistry,[8–11] and is thought to play a major role in the stratosphere by trapping Cl as HCl.[8,12]

$$HO_2 + Cl \rightarrow HCl + O_2 \quad (1)$$

[a]*Shaanxi Key Laboratory of Catalysis, School of Chemical & Environment Science, Shaanxi University of Technology, Hanzhong, Shaanxi 723001, P. R. China. E-mail: ztianlei88@l63.com; Fax: +86-0916-2641083; Tel: +86-0916-2641083*

[b]*School of Materials Science and Engineering, Guizhou Minzu University, Guiyang 550025, P. R. China. E-mail: longbo@gzmu.edu.cn*

[c]*Key Laboratory for Macromolecular Science of Shaanxi Province, School of Chemistry & Chemical Engineering, Shaanxi Normal University, Xi'an, Shaanxi 710062, P. R. China. E-mail: wlwang@snnu.edu.cn*

[d]*Shanghai Key Laboratory of Molecular Catalysis and Innovative Materials, Fudan University, Shanghai 200433, P. R. China*

† Electronic supplementary information (ESI) available. See DOI: 10.1039/c9ra03541a

‡ Yongqi Zhang, Mingjie Wen, and Zhuo Tang contributed equally to this work.

The potential importance of the Cl reaction with the HO_2 radical has led to a number of publications and, as a result, the kinetics of the HO_2 + Cl reaction have been studied experimentally for a range of temperatures.[8,13–16] Lee *et al.*[16] measured the rate constant of eqn (1) in a discharge-flow system with far infrared laser magnetic resonance within the temperature range 250–420 K. Similarly, Dobis *et al.*[8] used mass spectrometry to measure the rate constant ($(4.45 \pm 0.06) \times 10^{-11}$ cm^3 per molecule per s) of the reaction of eqn (1) in the temperature range 243–368 K. Both of these investigations showed that the rate constant in eqn (1) does not change within the measured temperature range. In another experiment, Hickson *et al.*[9] used the discharge-flow resonance fluorescence technique coupled with infrared diode laser spectroscopy to measure the rate constant for the reaction in eqn (1) within the temperature range 226–336 K. Their results show that the rate constant in eqn (1) derived from kinetic experiments expressed in Arrhenius form was $(1.6 \pm 0.2) \times 10^{-11} \exp[(249 \pm 34)/T]$ cm^3 per molecule per s. The theoretical aspect of the kinetics and mechanism for the reaction of eqn (1) have not yet been investigated. Thus, in this study, the reaction in eqn (1) has been investigated for the first time. These investigations provide meaningful information about the mechanisms and kinetics for the HO_2 + Cl reaction under atmospheric conditions. However, this effort has focused only on the non-catalytic process of the HO_2 + Cl reaction.

Water has long been considered a subject of chemical interest due to its abundance and unique properties in atmospheric chemistry.[17] It not only forms the hydrogen-bonded complexes ($HO_2\cdots H_2O$ and $H_2O\cdots HO_2$) with the HO_2 radical,[18–22] but can also actively participate in atmospheric reactions as a catalyst,[23,24] where an interesting result[20] is that the HO_2 self-reaction can be up to three times faster in the presence of water. Moreover, many previous studies have appeared in the literature on the electronic structure of the cluster $H_2O\cdots Cl$.[25,26] These situations have stimulated our interest in modeling the gas-phase reaction of the $H_2O\cdots HO_2\cdots$ Cl ternary system, in which a single water molecule serves as a catalyst.

Similar to the water monomer (WM), ammonia (AM) also exists widely in the atmosphere: its atmospheric concentration was found to be 30 ppb in a polluted ambient atmosphere and as high as 10 ppm in dairy farms.[27,28] As the most abundant alkaline component in the atmosphere, AM can also catalyze hydrogen abstraction reactions.[29,30] For example, AM plays an important role in the atmospheric formation of sulfuric acid (SA) through the hydrolysis of SO_3.[30] Compared to water, which is known to reduce the barrier of this reaction to 5.9 kcal mol^{-1}, AM makes the reaction barrierless and the value of its rate constant was found theoretically to be $\sim 10^5$ to 10^7 times that of a water catalyst. The above facts indicate that one cannot ignore AM in modeling different atmospheric hydrogen atom transfer (HAT) reactions. Meanwhile, to observe how an acid can influence the reaction in comparison to a neutral or a basic catalyst, the reaction in eqn (1) in the presence of formic acid (FA) as a catalyst has also been carried out.[31] In fact, FA can remarkably decrease the energy barrier of the HAT reaction, and is the reason in eqn (1) for considering FA as an acidic catalyst. It not only has significant abundance in the atmosphere, but it has also been found that FA can decrease the energy barrier significantly for several atmospheric HAT reactions.[31–35] The other issue is that it is known that a particular HAT reaction could show completely opposite temperature dependence in the presence of different catalysts. As temperature changes appreciably (by more than 100 K) within the troposphere, one needs to incorporate various types of catalysts to present a reliable picture of a particular reaction at various altitudes in the troposphere. In the troposphere, temperature decreases with increasing altitude. Therefore, with a change in altitude, the efficiency of acidic, neutral and basic catalysts on the reaction of eqn (1) should also be extensively investigated in order to provide a complete altitude dependence of the reaction.

In the present article, quantum chemical calculations have been performed to study the effect of acidic (FA), neutral (WM) and basic (AM) catalysts on the energetic and kinetic aspects of the HO_2 + Cl reaction. Then, the ways in which the relative impacts of catalysts and competition between the pathways are modulated with a change in tropospheric conditions have also been investigated extensively by considering the temperature dependence of rate constants and the altitude dependence of catalyst concentrations.

2. Computational details

2.1 Electronic structure calculations

The molecular geometries of the reactants, products, pre-reactive complexes, transition states, and post-reactive complexes for the oxidation of HO_2 by the Cl radical without and with catalyst molecules were optimized using the M06-2X functional[36,37] with the 6-311++G(2d,2p) basis set. The M06-2X functional is one of the best functionals with which to study noncovalent interactions[38,39] and has shown promising applications for estimating the thermochemistry and equilibrium structures for atmospheric reactions and molecular clusters.[40–42] At the M06-2X/6-311++G(2d,2p) level, the harmonic vibrational frequencies were calculated to verify the nature of the corresponding stationary points (minima or transition state) to provide the zero-point vibrational energy (ZPE) and to determine the thermodynamic contributions to the enthalpy and free energy. In addition, intrinsic reaction coordinate (IRC)[43–45] calculations were carried out to ensure that the transition states were connected to the desired reactants and products. Geometrical and frequency calculations were performed using Gaussian 09.[46] The final energies were obtained by performing single-point energy calculations at the CCSD(T)-F12A/VDZ-F12 (ref. 47–49) level of theory, based on the optimized geometries at the M06-2X/6-311++G(2d,2p) level, using ORCA.[50] It should be noted that the HO_2 + Cl reaction is a radical–radical reaction. It is likely that there are some multireference features in the HO_2 + Cl reaction. Post-CCSD(T) calculations are required for obtaining quantitative barrier heights, as has been reported in the literature.[51–53] However, we mainly focus on the effects of water clusters on the HO_2 + Cl reaction. Additionally, the calculated rate constant of the HO_2 + Cl reaction agrees well with the

experimental data. Thus, we have not considered post-CCSD(T) calculations.

2.2 Rate constant calculations

To estimate the effect of the catalyst (WM, AM and FA) added, theoretical rate constants of canonical variational transition (CVT)[54] state theory with small curvature tunneling (SCT) correction[55] for oxidation of HO_2 by a Cl radical without and with a catalyst were calculated by employing the Polyrate 8.2 program[56] coupled with the steady state approximation. As described in eqn (2), all the processes for oxidation of HO_2 by a Cl radical without and with a catalyst involve two major steps, as follows.

$$\text{Step a}: \text{A} + \text{B} \underset{k_{-1}}{\overset{k_1}{\rightleftharpoons}} \text{C}$$

$$\text{Step b}: \text{C} + \text{D} \underset{k_{-2}}{\overset{k_2}{\rightleftharpoons}} \text{E} \xrightarrow{k_{\text{uni}}} \text{F}$$

Here, A and B are any two among HO_2, Cl and a catalyst (WM, AM or FA), C is the binary complex formed by A and B. D is the remaining third species other than A and B. E is the ternary complex formed by HO_2, Cl and a catalyst. In step a, A combines with B to form an adduct C, whereas step b consists of two elementary processes: in the first process, C reacts with D to form E and subsequently E undergoes a unimolecular transformation to produce formation F *via* the corresponding TS.

Assuming that intermediate E was in equilibrium with the corresponding reactants (C and D) and was at steady state,[57] the rate constant for step b can be written as:

$$k_b = K_{eq_2} k_{uni} \quad (2)$$

The rate constant k_{uni} in eqn (2) has been evaluated by employing Polyrate 8.2 programs[56] in the framework of canonical variational transition state theory (CVT).[54] To include the tunneling effects for motion along the reaction coordinate for the title reactions at the CCSD(T)-F12A/VDZ-F12 (ref. 47–49)//M06-2X/6-311++G(2d,2p) level, the small curvature tunneling[55] (SCT) approximation has been adopted in this study. In addition, K_{eq_2} in eqn (2) was given by eqn (3).

$$K_{eq_2}(T) = \sigma \frac{Q_E}{Q_C Q_D} \exp\left(\frac{E_D + E_C - E_E}{RT}\right) \quad (3)$$

In eqn (3), the various Q values denote the partition functions of intermediate E, and reactants C and D, respectively. All partition functions were obtained using the M06-2X/6-311++G(2d,2p) method. E_D, E_C and E_E stand for the energies of the species of D, C and E, respectively; σ is the symmetry factor. In the present work, k_b has been used to compare the rates between the bare reaction and catalyzed reactions.

2.3 Effective rate constant calculations

If one incorporates the effect of step a, the resultant rate constant (k_t) can be written as:

$$k_t = K_{eq_1} K_{eq_2} k_{uni} \quad (4)$$

where K_{eq_1} stands for the equilibrium constant in step a, given by eqn (5).

$$K_{eq_1}(T) = \sigma \frac{Q_C}{Q_A Q_B} \exp\left(\frac{E_A + E_B - E_C}{RT}\right) \quad (5)$$

In eqn (5), the various Q values denote the partition functions of complex C, and reactants A and B, respectively. E_A, E_B and E_C stand for the energies of the species A, B and C, respectively. From the above, the rate of the reaction (v) in the presence of catalysts can be written as:

$$v = K_{eq_1} K_{eq_2} k_{uni}[A][B][D] = k_t[A][B][D] = k'_t[A][B] \quad (6)$$

k'_t is the effective rate constant, which could be considered a measure of the relative efficiencies of the different catalysts under atmospheric conditions, as it includes the concentration as well as rate constant of a particular catalyst.

3. Results and discussion

The transition state in each reaction channel was denoted by "TS" followed by a number, and the pre-reactive complex was denoted by "IM" followed by a number. The letter "a" was used to distinguish the transition states and pre-reactive complexes which are conformers of each other and therefore have the same features; species in the presence of WM, AM and FA were respectively denoted by "WM", "AM", and "FA" suffixes.

3.1 Uncatalyzed mechanism and kinetic for the HO_2 + Cl → HCl + O_2 reaction

The reactions between HO_2 and Cl on both singlet and triplet potential energy surfaces (PESs) have been investigated at the CCSD(T)-F12A/VDZ-F12//M06-2X/6-311++G(2d,2p) level in this study, where the channels of HCl + $^1O_2$ formation (singlet PES) and HCl + $^3O_2$ formation (triplet PES) have been considered, as shown in Fig. 1 and S2.† Moreover, compared with the two channels, it was found that the channel of HCl + $^3O_2$ formation on the triplet potential energy is the most favorable channel. In this study, we reinvestigated the channel of HCl + $^3O_2$ formation to determine the reliability of the theoretical methods used here and the catalytic effect of WM, AM and FA.

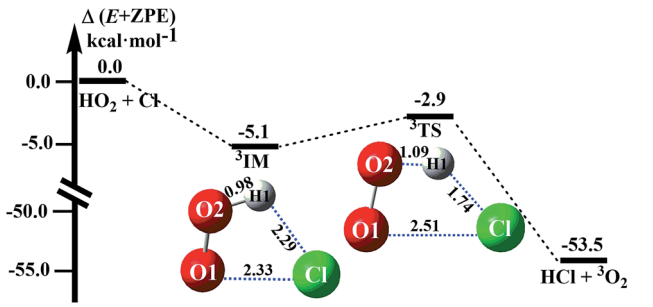

Fig. 1 Schematic energy diagrams of the HO_2 + Cl → HCl + $^3O_2$ reaction.

In absence of any catalyst, HO_2 first combines with Cl to produce a pre-reactive complex IM which is 5.1 kcal mol^{-1} more stable than isolated monomers (as shown in Fig. 1). Thereafter, complex IM undergoes a unimolecular transformation through cyclic TS with an energy barrier of 2.2 kcal mol^{-1}. The ΔH (298 K) of the $HO_2 + Cl \rightarrow HCl + O_2$ reaction was predicted to be -54.2 kcal mol^{-1}, which is in good agreement with the experimental estimates of -54.4 ± 0.8 kcal mol^{-1}.[9]

For the $HO_2 + Cl \rightarrow HCl + O_2$ reaction without water, Table 1 lists its CVT/SCT rate constant. As given in Table 1, at 213 and 320 K the rate constant was increased by 27% and 49% due to tunneling, while the rate constant was decreased to 12% and 34% due to recrossing effects. So, similar to previous investigations,[22,58,59] the tunneling transmission coefficients are very large for the hydrogen atom transfer process. Thus, herein the computed CVT/SCT rate constants have been used to estimate the catalytic effect of catalysts (WM, AM and FA). Additionally, Table 1 shows the computed CVT/SCT rate constants for Channel R1 (k_{R1}). It is worth noting that the rate constants of the $HO_2 + Cl \rightarrow HCl + O_2$ reaction increased with an increase in temperature. At 298 K, the calculated value of k_{R1} was 6.27×10^{-11} cm^3 per molecule per s, which is in good agreement with experimental reports.[8] So, this indicates that the calculations for the $HO_2 + Cl \rightarrow HCl + O_2$ reaction without and with catalysts at the CCSD(T)-F12A/VDZ-F12//M06-2X/6-311++G(2d,2p) level of theory are acceptable.

3.2 Mechanism and kinetics of the H_2O catalyzed $HO_2 + Cl \rightarrow HCl + O_2$ reaction

In the presence of a water molecule, both bodies of HO_2 and Cl can respectively interact with water to form two-body complexes first in the entrance channels before interacting with the third body of Cl or HO_2. So, it is very necessary to find the stable configurations of the two-body complexes between HO_2 (or Cl) and H_2O. In order to find all possible stable configurations of these complexes, global minimum searching of geometric structures was carried out using Tsinghua Global Minimum (TGMin).[60,61] Then the initial structures were selected for geometrical optimization using the M06-2X/6-31G(d,p) method. The isomer structures within 5.0 kcal mol^{-1} of the global minimum were re-optimized by the M06-2X/6-311++G(2d,2p) method. As shown in Fig. 2 and S3,† and consistent with previous reports,[62–66] a five-membered ring complex $H_2O\cdots HO_2$ is much more stable than the single hydrogen bond (or van der Waals interaction) complexes $HO_2\cdots H_2O$, $H_2O\cdots Cl$ and $Cl\cdots H_2O$ with its binding energy being larger by 5.1–6.1 kcal mol^{-1}. Meanwhile, the equilibrium constants of these complexes at 298 K are 6.05×10^{-20}, 2.60×10^{-22}, 1.93×10^{-21} and 3.85×10^{-21} cm^3 per molecule, respectively (Table S3†). Considering typical tropospheric concentrations of 7.64×10^{17} molecules per cm^3 of H_2O, 3×10^8 molecules per cm^3 of HO_2 (ref. 67) and 3×10^5 molecules per cm^3 of Cl,[68,69] the atmospheric concentration of the $H_2O\cdots HO_2$ complex has been estimated to be 1.39×10^7 molecules per cm^3, which is 2.33×10^2, 3.14×10^4 and 1.58×10^4 times the concentrations of $HO_2\cdots H_2O$, $H_2O\cdots Cl$ and $Cl\cdots H_2O$. Thus, in the four bimolecular reactions of eqn (7)–(10), we can predict that the atmospheric relevance of the bimolecular reaction of eqn (7) will be much more obvious than those reactions of eqn (8)–(10). However, for comparison, the potential energy surfaces (PESs) for all four possible types of bimolecular reactions have been considered.

$$H_2O\cdots HO_2 + Cl \rightarrow H_2O\cdots HCl + O_2 \quad (7)$$

$$HO_2\cdots H_2O + Cl \rightarrow H_2O + HCl + O_2 \quad (8)$$

$$Cl\cdots H_2O + HO_2 \rightarrow H_2O\cdots HCl + O_2 \quad (9)$$

$$H_2O\cdots Cl + HO_2 \rightarrow H_2O\cdots HCl + O_2 \quad (10)$$

Fig. 3 presents the potential energy surfaces (PESs) for the water-catalyzed $HO_2 + Cl \rightarrow H_2O + {}^3O_2$ reaction (Channels RWM1, RWM2 and RWM3), along with the local minimum geometries on the corresponding reaction pathways. In Fig. 3,

Table 1 The equilibrium constants (molecules per cm^3) and rate constants (cm^3 per molecule per s) for the main reaction of the $HO_2 + Cl \rightarrow HCl + {}^3O_2$ reaction within the temperature range 213–320 K[a]

T (K)	I^{CVT}	κ^{SCT}	K_{eq}	k_2^{TST}	k_2^{CVT}	$k_2^{CVT/SCT}$	k_R	k_{exp}
213	0.12	15.27	1.07×10^{-21}	1.94×10^{11}	2.43×10^{10}	3.70×10^{11}	3.98×10^{-10}	
216	0.13	14.33	9.61×10^{-22}	2.01×10^{11}	2.63×10^{10}	3.77×10^{11}	3.62×10^{-10}	
219	0.14	13.47	8.63×10^{-22}	2.08×10^{11}	2.85×10^{10}	3.84×10^{11}	3.31×10^{-10}	
224	0.15	12.19	7.26×10^{-22}	2.19×10^{11}	3.23×10^{10}	3.94×10^{11}	2.86×10^{-10}	
230	0.16	10.89	5.96×10^{-22}	2.34×10^{11}	3.74×10^{10}	4.07×10^{11}	2.43×10^{-10}	
235	0.17	9.96	5.10×10^{-22}	2.46×10^{11}	4.20×10^{10}	4.18×10^{11}	2.13×10^{-10}	
250	0.20	7.79	3.31×10^{-22}	2.85×10^{11}	5.78×10^{10}	4.50×10^{11}	1.49×10^{-10}	
259	0.22	6.82	2.62×10^{-22}	3.10×10^{11}	6.88×10^{10}	4.69×10^{11}	1.23×10^{-10}	
280	0.27	5.20	1.62×10^{-22}	3.72×10^{11}	9.90×10^{10}	5.15×10^{11}	8.32×10^{-11}	
290	0.29	4.65	1.32×10^{-22}	4.04×10^{11}	1.16×10^{11}	5.37×10^{11}	7.08×10^{-11}	
298	0.30	4.28	1.13×10^{-22}	4.30×10^{11}	1.30×10^{11}	5.55×10^{11}	6.27×10^{-11}	$((4.45 \pm 0.06) \times 10^{-11})^b$
300	0.31	4.19	1.09×10^{-22}	4.37×10^{11}	1.34×10^{11}	5.60×10^{11}	6.09×10^{-11}	
310	0.33	3.81	9.11×10^{-23}	4.71×10^{11}	1.53×10^{11}	5.83×10^{11}	5.32×10^{-11}	
320	0.34	3.49	7.72×10^{-23}	5.06×10^{11}	1.74×10^{11}	6.07×10^{11}	4.69×10^{-11}	

[a] k_R is the rate constant of $HO_2 + Cl \rightarrow HCl + {}^3O_2$. [b] The experimental value from ref. 8.

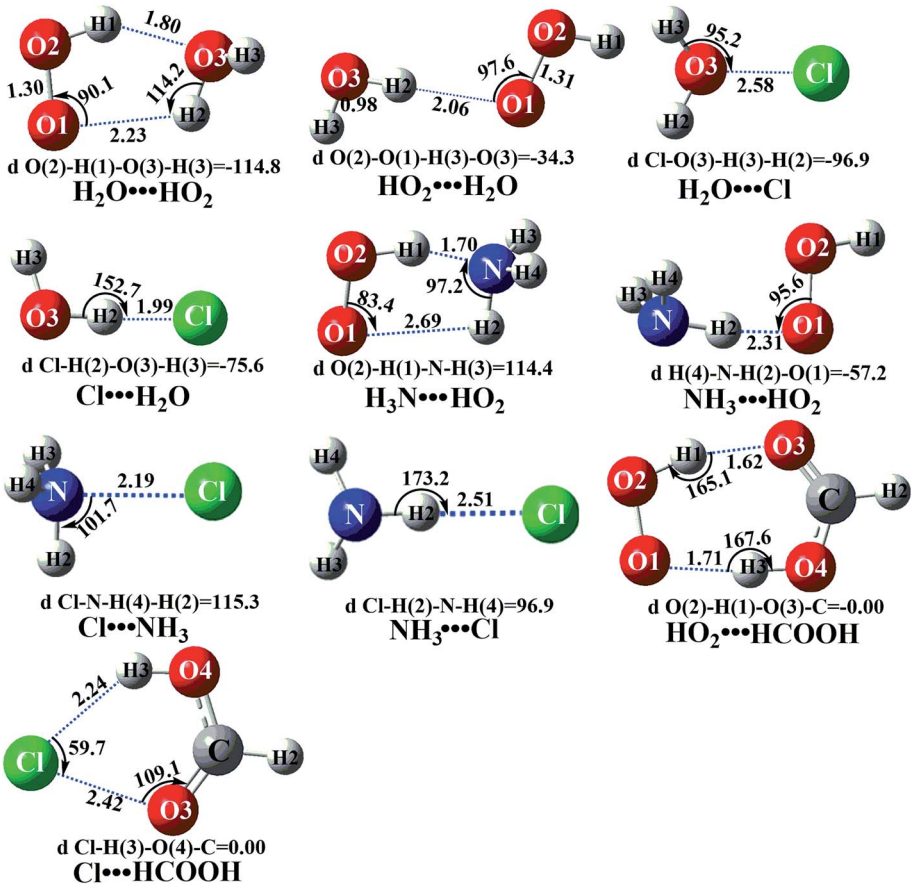

Fig. 2 Optimized geometries of the reactions of the most advantageous complexes for the HO_2 + Cl → HCl + $^3O_2$ reaction with catalyst X (X = H_2O, NH_3, HCOOH) at the M06-2X/6-311++G(2d,2p) level of theory.

the $H_2O\cdots HO_2$ + Cl reaction is mechanistically different from the three other reactions of $HO_2\cdots H_2O$ + Cl, $Cl\cdots H_2O$ + HO_2 and $H_2O\cdots Cl$ + HO_2, as the $H_2O\cdots HO_2$ + Cl reaction involves a stepwise route, whereas the other reactions involve one elementary step. During the stepwise route reaction, the reaction occurs first *via* a ring enlargement, and then proceeds through a hydrogen abstraction mechanism, whereas in the case of the one elementary step reaction channel, the reaction proceeds through a hydrogen abstraction process alone.

For Channel RWM1, two kinds of reaction types can be taken (a) between $H_2O\cdots Cl$ and HO_2 or (b) between $H_2O\cdots HO_2$ and Cl. When the $H_2O\cdots Cl$ complex and HO_2 act as reactants, the reaction occurs in one elementary step, which is similar to the uncatalyzed reaction of HO_2 + Cl → HCl + O_2 above, the HCOOH-catalyzed hydrolysis of CH_3CHO and HCHO,[41,70] as well as the HNO_3 and HCOOH-catalyzed hydrolysis of SO_3.[71–73] The reaction starts with the formation of the pre-reactive complex IM_WM2, as described in Fig. 3. As shown in Fig. 3, the pre-reactive IM_WM2 complex has a six-membered ring structure, where there are two hydrogen-bonded interactions and a van der Waals interaction. The binding energy (9.5 kcal mol^{-1}) of IM_WM2 is about 7.5 kcal mol^{-1} lower than that of the $H_2O\cdots Cl$ and HO_2 reactants at the CCSD(T)-F12A/VDZ-F12//M06-2X/6-311++G(2d,2p) level. Following the formation of the pre-reactive complex IM_WM2, the reaction proceeded through transition state TS_WM2 to produce the product of $H_2O\cdots Cl–H$ + $^3O_2$ after climbing the barrier height of 7.2 kcal mol^{-1}. In transition state TS_WM2, the seven-membered ring structure was still conserved with the Cl radical abstracting the H atom of the HO_2 moiety in the $H_2O\cdots HO_2$ complex. When $H_2O\cdots HO_2$ and Cl act as reactants, Channel RWM1 occurs in two steps, as depicted in Fig. 3, which is similar to the H_2O-catalyzed reactions[66,74] of HO_2 + HO and HO_2 + HS. The first step begins with the formation of the pre-reactive IM_WM1 complex, which transforms into the IM_WM2 product through the TS_WM1 transition state *via* a ring enlargement, while the second step is IM_WM2 isomerization into $H_2O\cdots Cl–H$ + $^3O_2$ *via* TS_WM2, which was discussed above. Herein, we focus on the first step because the second step has been previously discussed in the $H_2O\cdots Cl$ and HO_2 reaction. It should be noted that IM_WM1 has a binding energy of 8.4 kcal mol^{-1}, which is about 1.1 kcal mol^{-1} higher than that of the corresponding complex IM_WM2 in the $H_2O\cdots Cl$ + HO_2 reaction. Furthermore, the energy barrier of IM_WM1 isomerization into IM_WM2 is very low with a value of 3.0 kcal mol^{-1}, revealing that this process occurs facilely in the atmosphere. In order to test whether the $H_2O\cdots Cl$ + HO_2 reaction is more favorable than the $H_2O\cdots HO_2$ + Cl reaction or not, the effective rate constants of these two routes in Channel

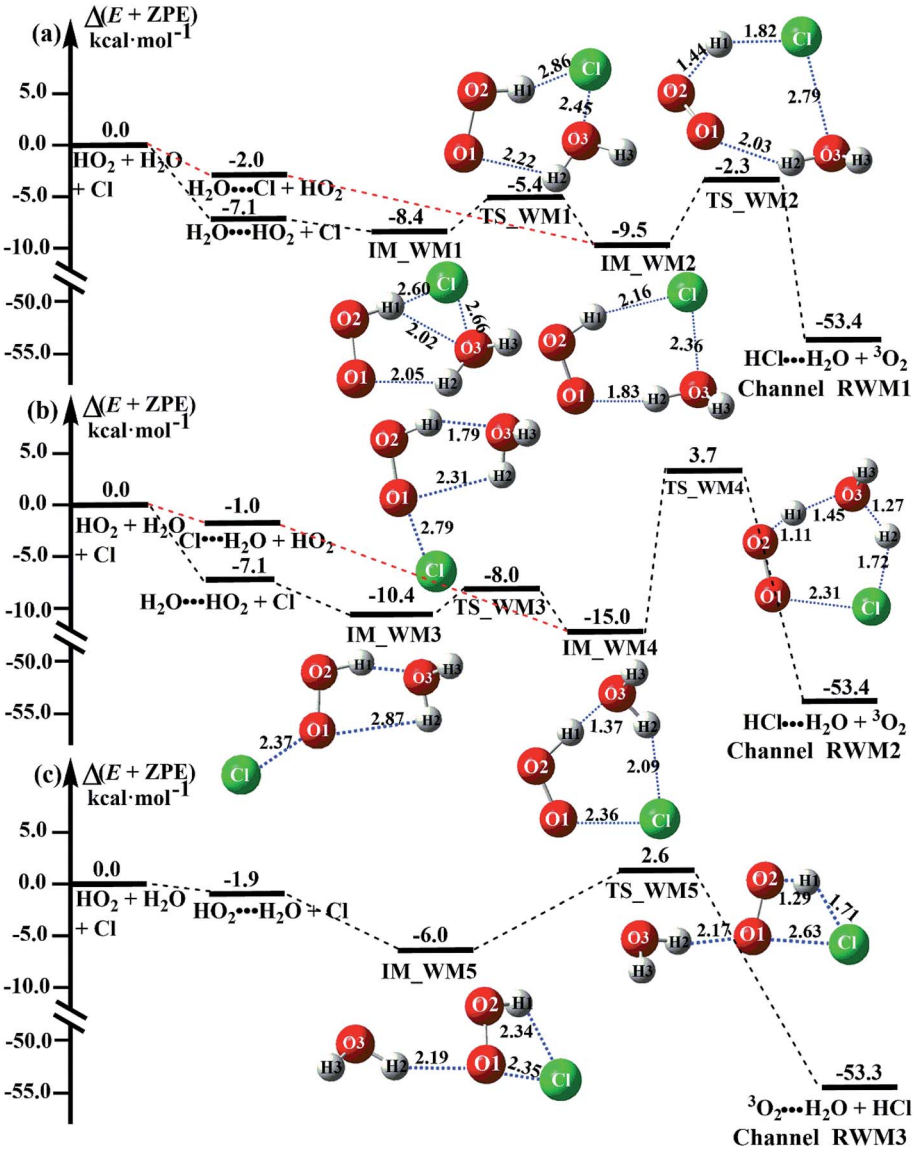

Fig. 3 Schematic energy diagrams of the HO_2 + Cl → HCl + $^3O_2$ reaction with catalyst H_2O at the CCSD(T)-F12A/VDZ-F12//M06-2X/6-311++G(2d,2p) level, including the zero-point energy correction (kcal mol^{-1}).

RWM1 were calculated in Table S7,† where the effective rate constants of the $H_2O\cdots Cl + HO_2$ and $H_2O\cdots HO_2$ + Cl reactions were respectively labeled as k_t'(RWM1_o) and k_t'(RWM1_s). It can be seen in Table S7† that the value of k_t'(RWM1_s) is much larger than that of k_t'(RWM1_o) because the rate constant ratio k_t'(RWM1_s)/k_t'(RWM1_o) is about 5.29×10^2 to 4.91×10^1 times higher within the temperature range 280–320 K, indicating that Channel RWM1 *via* the interaction between $H_2O\cdots HO_2$ and Cl is more favorable than that *via* $H_2O\cdots Cl$ interacting with HO_2.

As for Channel RWM2, two kinds of reaction types can be taken both by (a) the stepwise mechanism ($H_2O\cdots HO_2$ + Cl reaction) and (b) the one-step process ($Cl\cdots H_2O + HO_2$ reaction). Similar to Channel RWM1, the stepwise mechanism in Channel RWM2 is more favorable than that of the one-step process with its effective rate constant (k_t'(RWM2_s)) being 1087-52 times larger than the corresponding value (k_t'(RWM2_o)) of the latter process. Thus, for Channel RWM2, only the stepwise mechanism is discussed here. Regarding the stepwise mechanism of Channel RWM2, in the first step, similar to the ring enlargement from IM_WM1 to IM_WM2 in Channel RWM1, the five-membered ring complex IM_WM3 in Channel RWM2 was rearranged into a six-membered ring complex IM_WM4 through TS_WM3 with a barrier height of 2.4 kcal mol^{-1}. In the second step, following formation of IM_WM4, Channel RWM2 proceeded through transition state TS_WM4 to form $^3O_2$ and $H_2O\cdots H_2O$ with a barrier height of 18.7 kcal mol^{-1}. It is worth noting that the second step is the rate-determining step in both stepwise mechanisms of Channels RWM1 and RWM2. For the rate-determining step of Channels RWM1 and RWM2, unlike the transition state TS_WM2 in Channel RWM1 that involves a direct hydrogen abstraction, the transition state TS_WM4 in

Channel RWM2 contains a double hydrogen transfer mechanism, where water acts as a bridge for the hydrogen transfer from the HO_2 to the Cl radical, and as the WM accepts the hydrogen from HO_2, it simultaneously donates another hydrogen atom to the Cl radical. Such a discrepancy in mechanism between Channels RWM1 and RWM2 may lead to the energy of transition state TS_WM2 in Channel RWM1 being 6.0 kcal mol^{-1} lower than that of TS_WM4 in the latter reaction. Meanwhile, for the stepwise mechanism of Channels RWM1 and RWM2, the effective rate constant of Channel RWM1 (k'_t(RWM1_s)) is much larger than the corresponding value (k'_t(RWM2_s)) of Channel RWM2. This indicates that the double hydrogen transfer mechanism in Channel RWM2 is less favorable than the direct hydrogen abstraction involved in Channel RWM1. Such a discrepancy in mechanism between Channels RWM1 and RWM2 is consistent with our previous reports.[22,65,66,75]

Unlike Channels RWM1 and RWM2 above, which mainly involve a stepwise process, the $HO_2\cdots H_2O$ + Cl reaction (Channel RWM3) consists of a one-step mechanism. As for Channel RWM3, the reaction started with the formation of a four-membered ring pre-reactive hydrogen bond complex IM_WM5 with a binding energy of 6.0 kcal mol^{-1}. Starting from IM_WM5, Channel RWM3 proceeded through transition state TS_WM5 with a barrier height of 2.6 kcal mol^{-1}, which is similar in structure to the naked transition state TS, where the Cl radical directly abstracted the hydrogen of HO_2. The effective rate constant of Channel RWM3 (k'_t(RWM3)) listed in Table S7† is lower by 7–8 orders than the corresponding value of k'_t(RWM1_s) in Channel RWM1 ($H_2O\cdots HO_2$ + Cl reaction). As a result of the above findings of HCl + $^3O_2$ formation with H_2O, the atmospheric relevance of the $H_2O\cdots HO_2$ + Cl reaction occurring through direct hydrogen abstraction was found to be most obvious in the H_2O catalyzed HO_2 + Cl → HCl + $^3O_2$ reaction.

3.3 Mechanism and kinetics of the NH_3 catalyzed HO_2 + Cl → HCl + O_2 reaction

As shown in Fig. 4, there are still four bimolecular reactions (eqn (11)–(14)) in the NH_3 catalyzed HO_2 + Cl → HCl + O_2 reaction, where the $H_3N\cdots HO_2$ + Cl reaction involves a stepwise route, and the three other reactions of $Cl\cdots NH_3$ + HO_2, $NH_3\cdots Cl$ + HO_2 and $NH_3\cdots HO_2$ + Cl occur *via* one elementary step. Compared with the H_2O catalyzed reaction in Fig. 3, the NH_3 catalyzed reaction shown in Fig. 4 has the same mechanism, with NH_3 replacing H_2O.

$$H_3N\cdots HO_2 + Cl \rightarrow HCl\cdots NH_3 + {}^3O_2 \quad (11)$$

$$Cl\cdots NH_3 + HO_2 \rightarrow HCl\cdots NH_3 + {}^3O_2 \quad (12)$$

$$NH_3\cdots Cl + HO_2 \rightarrow HCl\cdots NH_3 + {}^3O_2 \quad (13)$$

$$NH_3\cdots HO_2 + Cl \rightarrow {}^3O_2\cdots NH_3 + HCl \quad (14)$$

Similar to the $H_2O\cdots HO_2$ complex, the $H_3N\cdots HO_2$ complex, as shown in Fig. 2, also forms a five-membered ring-like structure *via* the formation of two hydrogen bonds, where both HO_2 radical and NH_3 act as hydrogen donor or acceptor or both simultaneously, as shown in Fig. 2. The binding energy of $H_3N\cdots HO_2$ is 9.8 kcal mol^{-1}, which is larger by 2.7 kcal mol^{-1} than that of the $H_2O\cdots HO_2$ complex. Single hydrogen bond (or van der Waals interaction) complexes of $HO_2\cdots H_3N$, $Cl\cdots H_3N$ and $H_3N\cdots Cl$ are less stable than $H_3N\cdots HO_2$. As shown in Table S3,† the atmospheric concentration of the $H_3N\cdots HO_2$ complex is 1.26×10^5 molecules per cm^3, which is 1.93×10^5, 1.83×10^3 and 1.25×10^9 times larger than the concentrations of complexes $NH_3\cdots HO_2$, $Cl\cdots H_3N$ and $NH_3\cdots Cl$. Thus, in the four bimolecular reactions of eqn (11)–(14), we predict that the atmospheric relevance of the bimolecular reaction of eqn (11) ($H_3N\cdots HO_2$ + Cl reaction) will be much more obvious than the relevance of the reactions of eqn (12)–(14). This is similar to the water-catalyzed reactions in eqn (7)–(10) where the $H_2O\cdots HO_2$ + Cl reaction is the most favorable in the H_2O catalyzed HO_2 + Cl → HCl + $^3O_2$ reaction. This prediction has been proved by the calculated effective rate constants listed in Table S7,† where the effective rate constants of the $H_3N\cdots HO_2$ + Cl reaction occurring through Channel RAM1 (k'_t(RAM1_s)) and Channel RAM2 (k'_t(RAM2_s)) are much larger than the corresponding one-step reactions of $Cl\cdots NH_3$ + HO_2 (k'_t(RAM1_o)) and $NH_3\cdots Cl$ + HO_2 (k'_t(RAM2_o)). Meanwhile, the values both (k'_t(RAM1_s)) and (k'_t(RAM2_s)) are larger than the values of k'_t(RAM3) ($NH_3\cdots HO_2$ + Cl reaction). Thus, only the reaction of $H_3N\cdots HO_2$ + Cl has been considered here.

As shown in Fig. 4, for the $H_3N\cdots HO_2$ + Cl reaction, the stepwise mechanism occurring through Channel RAM1 is different from that *via* Channel RAM2 in three aspects. First, the ring enlargement in Channel RAM1 occurs more easily than that in Channel RAM2 with its barrier lower by 1.2 kcal mol^{-1}. Secondly, from the geometrical point of view, complexes IM_AM2 and IM_AM4 are different, because Cl and NH_3 have exchanged positions in these two complexes. This is possibly the reason why complex IM_AM2 is more stable by 10.5 kcal mol^{-1} than complex IM_AM4. The third reason is that the barrier height of the rate-determining step in Channel RAM1 is lower by 7.5 kcal mol^{-1} than that in Channel RAM2. The calculated values of the effective rate constant for the $H_3N\cdots HO_2$ + Cl reaction at various temperatures are given in Table S7.† As listed in Table S7,† the effective rate constant of the $H_3N\cdots HO_2$ + Cl reaction occurring through Channel RAM1 (k'_t(RAM1_s)) is larger by 10^2 to 10^3 times than that occurring through Channel RAM2 (k'_t(RAM2_s)), indicating that the stepwise route of the $H_3N\cdots HO_2$ + Cl reaction occurs mainly through direct hydrogen abstraction, which is similar to the $H_2O\cdots HO_2$ + Cl reaction in Fig. 3.

3.4 Mechanism and kinetics of the HCOOH-catalyzed HO_2 + Cl → HCl + O_2 reaction

The formic acid catalyzed reaction channels also follow a similar trend to that found in the cases of H_2O and NH_3. Depending upon the bimolecular complexes here, the two

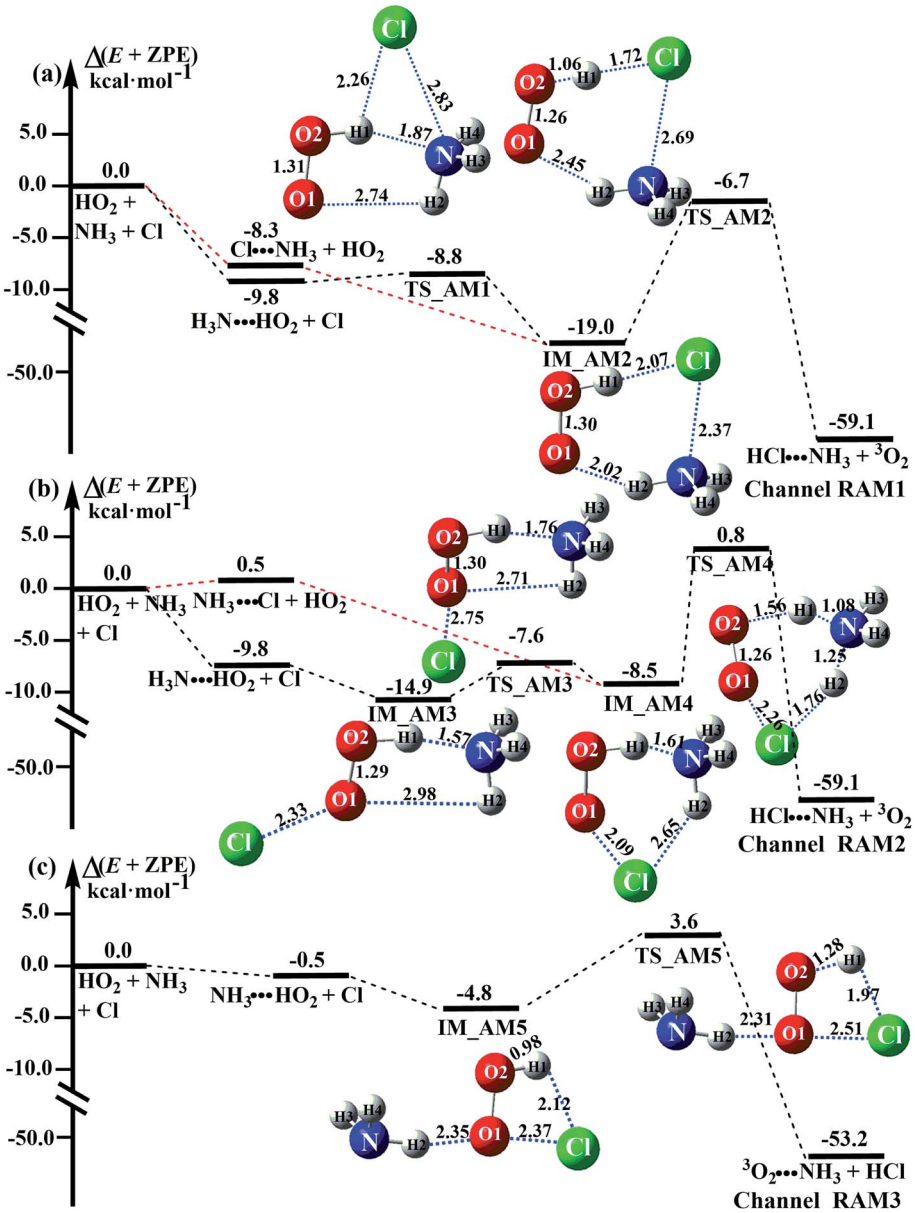

Fig. 4 Schematic energy diagrams of the HO_2 + Cl → HCl + $^3O_2$ reaction with catalyst NH_3 at the CCSD(T)-F12A/VDZ-F12//M06-2X/6-311++G(2d,2p) level, including the zero-point energy correction (kcal mol^{-1}).

different types of reactions seen in Fig. 5 are possible. One is the reaction between the HO_2···HCOOH complex and the Cl radical, the other is the reaction between the Cl···HCOOH complex and the HO_2 radical. It is important to note that the HO_2···HCOOH and Cl···HCOOH complexes shown in Fig. 2 are respectively the most stable complexes between HCOOH and HO_2 (or Cl) with their binding energies being larger by 5.6 to 8.6 and 2.9–3.0 kcal mol^{-1}, respectively, than those of other corresponding bimolecular complexes. Meanwhile, the atmospheric concentrations of the HO_2···HCOOH and Cl···HCOOH complexes are 1.49×10^4 and 1.48×10^{-3} molecules per cm^3, respectively, which are 2.03×10^3 to 2.43×10^3 and 1.32×10^1 to 3.47×10^1, respectively, times larger than the other complex between HCOOH and HO_2 (or Cl). This indicates that the atmospheric relevance of the two types of reactions here will be most obvious in the HCOOH catalyzed HO_2 + Cl → HCl + $^3O_2$ reaction.

As shown in Fig. 5, the HO_2···HCOOH + Cl reaction consists of a stepwise mechanism, where the reaction occurs *via* a ring enlargement from the seven-membered ring complex IM_ FA1 (or IM_ FA3) to the eight-membered ring complex IM_ FA2 (or IM_ FA4) first and then it proceeds through a hydrogen abstraction mechanism; whereas the one-step route of the Cl··· HCOOH + HO_2 reaction occurs with only a hydrogen abstraction mechanism being involved. Table S7† also lists the effective rate constants of the HO_2···HCOOH + Cl and Cl···HCOOH + HO_2 reactions within the temperature range 280–320 K. As shown in Table S7,† for Channel RFA1, the effective rate constant of the

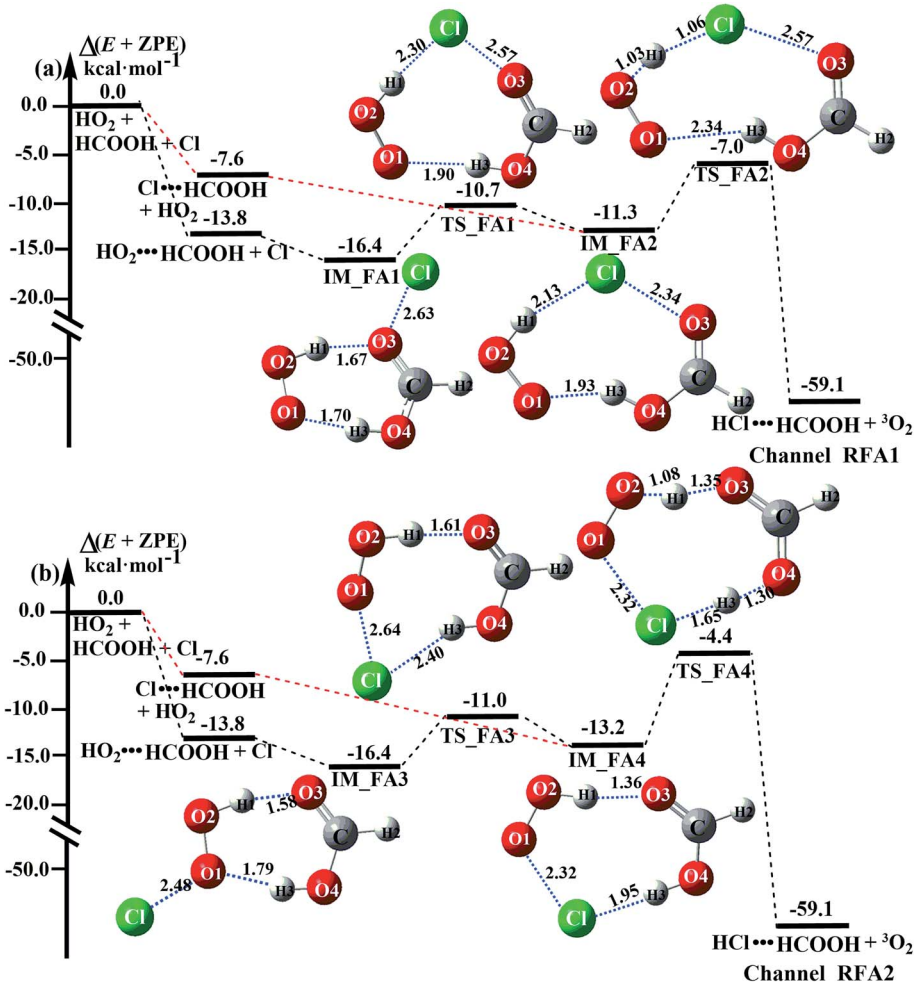

Fig. 5 Schematic energy diagrams of the HO_2 + Cl → HCl + $^3O_2$ reaction with catalyst HCOOH at the CCSD(T)-F12A/VDZ-F12//M06-2X/6-311++G(2d,2p) level, including the zero-point energy correction (kcal mol^{-1}).

stepwise mechanism (k_t'(RFA1_s)) is larger by 2–4 orders of magnitude than that of the one-step route (k_t'(RFA1_o)). A similar result can be obtained in Channel RFA2, where the effective rate constant of stepwise mechanism (k_t'(RFA2_s)) is also larger by 4–5 orders of magnitude than that of the corresponding one-step route (k_t'(RFA2_o)). These results suggest that the stepwise reaction of HO_2···HCOOH + Cl is more favorable than that of the one-step route of the Cl···HCOOH + HO_2 reaction.

Similar to the H_2O···HO_2 + Cl and H_3N···HO_2 + Cl reactions above, as shown in Fig. 5, for the HO_2···HCOOH + Cl reaction, the second step in both Channels RFA1 and RFA2 is the rate-determining step. For the rate-determining step of the HO_2···HCOOH + Cl reaction, the barrier height of direct hydrogen abstraction in Channel RFA1 is lower by 2.6 kcal mol^{-1} than that of the double hydrogen transfer mechanism in Channel RFA2. Meanwhile, the effective rate constant of the HO_2···HCOOH + Cl reaction occurring through Channel RFA1 (k_t'(RFA1_s)) is 1.84×10^1 to 2.41×10^1 times larger than that occurring through Channel RFA2 (k_t'(RFA2_s)), indicating that the stepwise route of the HO_2···HCOOH + Cl reaction occurs mainly through direct hydrogen abstraction, and the double hydrogen transfer mechanism in the HO_2···HCOOH + Cl reaction can be neglected, which is similar to the H_2O···HO_2 + Cl reaction in Fig. 3 and the H_3N···HO_2 + Cl reaction in Fig. 4.

3.5 Atmospheric relevance of the HO_2 + Cl → HCl + O_2 reaction with H_2O, NH_3 and HCOOH

Since the mechanisms and kinetics mentioned above showed that the stepwise mechanism of the X···HO_2 (X = WM, AM, and FA) + Cl reaction is the favorable route for HO_2 + Cl → HCl + O_2 with catalyst X, another main aim of our work was to study the influence of catalyst X on the HO_2 + Cl → HCl + O_2 reaction under atmospheric conditions. Thus, the rate constants for the HO_2 + Cl → HCl + O_2 reaction, the effective rate constant of the X···HO_2 + Cl reaction occurring through direct hydrogen abstraction as well as the rate ratio between the reaction with a catalyst and the reaction without a catalyst have been listed in Tables 2 and 3.

3.5.1 0 km altitude within the temperature range 280–320 K. Due to the fact that the concentration of WM varies depending on relative humidity (RH), at 0 km altitude, the WM

Table 2 Effective rate constants (cm^3 per molecule per s) of the X···HO_2 + Cl reaction occurring through direct hydrogen abstraction as well as the rate ratio between the reaction with a catalyst and the reaction without a catalyst X (X = H_2O, NH_3, HCOOH) within the temperature range 280–320 K at 0 km altitude[a]

	k'_t(RAM1_s)			k'_t(RFA1_s)							
T/K	k'_t(RWM1_s) 100%	(10 ppbv)	(2900 ppbv)	Average	High	k'_t(RWM1_s)/k_R	k'_t(RAM1_s)$_{10ppbv}$/k_R	k'_t(RAM1_s)$_{2900ppbv}$/k_R	k'_t(RFA1_s)$_{Average}$/k_R	k'_t(RFA1_s)$_{High}$/k_R
280	2.64×10^{-13}	3.67×10^{-18}	1.07×10^{-15}	2.38×10^{-14}	3.09×10^{-13}	0.32%	0.00%	0.00%	0.03%	0.37%
290	2.67×10^{-13}	3.08×10^{-18}	8.99×10^{-16}	7.71×10^{-15}	1.02×10^{-13}	0.38%	0.00%	0.00%	0.01%	0.14%
298	2.90×10^{-13}	1.09×10^{-19}	3.08×10^{-16}	3.48×10^{-15}	4.40×10^{-14}	0.46%	0.00%	0.00%	0.01%	0.07%
300	3.40×10^{-13}	9.26×10^{-19}	2.74×10^{-16}	2.87×10^{-15}	3.62×10^{-14}	0.56%	0.00%	0.00%	0.00%	0.06%
310	3.08×10^{-13}	5.32×10^{-19}	1.53×10^{-16}	1.08×10^{-15}	1.44×10^{-14}	0.58%	0.00%	0.00%	0.00%	0.03%
320	2.52×10^{-13}	3.10×10^{-19}	9.03×10^{-17}	4.60×10^{-16}	5.88×10^{-15}	0.54%	0.00%	0.00%	0.00%	0.01%

[a] k'_t(RWM1_s) = k(RWM1_s)K_{eq}(H_2O···HO_2)[H_2O]; k'_t(RAM1_s) = k(RAM1_s)K_{eq}(H_3N···HO_2)[NH_3]; k'_t(RFA1_s) = k(RFA1_s)K_{eq}(HO_2···HCOOH)[HCOOH]. K_{eq}(H_2O···HO_2), K_{eq}(H_3N···HO_2) and K_{eq}(HO_2···HCOOH) are the equilibrium constants for the formation of the H_2O···HO_2, H_3N···HO_2 and HO_2···HCOOH complexes, respectively.

concentration between 20% (5.2×10^{16} to 4.1×10^{17} molecules per cm^3) and 100% (2.6×10^{17} to 2.3×10^{18} molecules per cm^3) RH has been considered[76] within the temperature range 280–320 K. Usually, at 0 km altitude, depending on various atmospheric conditions, AM varies from 0.1 (2.6×10^9 to 2.3×10^9 molecules per cm^3) to 10 (2.6×10^{11} to 2.3×10^{11} molecules per cm^3) ppbv within the temperature range 280–320 K.[77–79] However, under certain extreme conditions, the local concentration of AM has been found to reach as high as 2900 (7.6×10^{13} to 6.7×10^{13} molecules per cm^3) ppbv[80] within the temperature range 280–320 K, and this situation cannot be neglected. The concentration of FA at 0 km altitude varies from ~0.01 ppbv (2.6×10^8 to 2.3×10^8 molecules per cm^3) to ~10 ppbv (2.6×10^{11} to 2.3×10^{11} molecules per cm^3) depending upon the temperature and other parameters at zero km altitude within the temperature range 280–320 K.[81] Meanwhile, the average concentration of FA (2.0×10^{10} to 1.8×10^{10} molecules per cm^3) at 0 km altitude has been reported within the temperature range 280–320 K. The calculated k'_t values for various catalysts at different catalyst concentrations and temperatures are listed in Table 2. It is evident from Table 2 that FA (at a high concentration limit of 10 ppbv) completely dominates over all other catalysts at 280 K, whereas water (100% RH) completely dominates within the temperature range 290–320 K. As far as the basic catalyst (AM) is concerned, it is never the most efficient catalyst under any circumstances. In fact, k'_t for AM at 2900 ppbv concentration is lower than that for FA (average). As shown in Table S8,† this means that AM would not make any significant contribution in catalyzing the $HO_2 + Cl \rightarrow HCl + O_2$ reaction. In order to quantitatively assess the impact of FA (at a high concentration limit of 10 ppbv) and WM at 100% RH on the $HO_2 + Cl \rightarrow HCl + O_2$ reaction, the rate ratio between the reaction with a catalyst and without a catalyst is also listed in Table 2. The calculated results in Table 2 show that the rate ratio of k'_t(RWM1_s)/k_R and $k'_t(\text{RFA1\_s})_{High}/k_R$ is less than 0.6% within the temperature range 280–320 K, indicating that the $HO_2 + Cl \rightarrow HCl + O_2$ reaction with catalysts of H_2O, NH_3, and HCOOH cannot compete with the reaction without a catalyst.

3.5.2 Higher altitudes in the troposphere within the temperature range 213–298 K. The average concentrations of FA at 0, 5, 10 and 15 km altitudes are known to be 9.0×10^{10}, 2.0×10^{10}, 8.3×10^9 and 3.2×10^9 molecules per cm^3, respectively,[81,82] whereas the concentrations of WM were found to be 5.2×10^{17}, 2.4×10^{16}, 4.9×10^{15} and 2.0×10^{13} molecules per cm^3, respectively.[83] The concentrations of AM at 0, 5, 10 and 15 km altitude were found to be 2.46×10^{11}, 7.57×10^9, 8.48×10^8 and 1.24×10^8 molecules per cm^3, respectively.[76] Besides concentration of the catalysts, the temperature also changes appreciably with changing altitude in the troposphere. The average temperatures at 5, 10 and 15 km altitude are 259, 230 and 213 K, respectively.[76,84] The k'_t values were calculated for all the catalysts using the above-mentioned concentration and temperature values for altitudes up to 15 km and are given in Table 3. It is evident from Table 3 that at altitudes of 5, 10 and 15 km, neutral (WM) and basic catalysts (AM) do not match their acidic counterparts at higher altitudes and the gap between them increases monotonically with increasing altitude.

Table 3 Effective rate constants (cm^3 molecule per s) of the X···HO_2 + Cl reaction occurring through direct hydrogen abstraction as well as the rate ratio between the reaction with a catalyst and the reaction without a catalyst X (X = H_2O, NH_3, HCOOH) at various altitudes in the troposphere

Altitude	T (K)	k'_t(RWM1_s)	k'_t(RAM1_s)	k'_t(RFA1_s)	k'_t(RWM1_s)/k_R	k'_t(RAM1_s)/k_R	k'_t(RFA1_s)/k_R
0 km	298	1.96×10^{-13}	1.07×10^{-18}	1.65×10^{-14}	0.31%	0.00%	0.03%
5 km	259	2.09×10^{-13}	5.91×10^{-18}	3.04×10^{-13}	0.17%	0.00%	0.25%
10 km	230	1.33×10^{-12}	1.64×10^{-18}	1.02×10^{-11}	0.55%	0.00%	4.20%
15 km	213	2.68×10^{-14}	2.91×10^{-18}	9.63×10^{-11}	0.01%	0.00%	24.20%

This showed that at altitudes of 5, 10 and 15 km, the catalytic effect of FA is higher those of catalysts of WM and AM, respectively. For catalyst FA, as k'_t incorporates both rate coefficient (termolecular rate coefficients (k_t), as seen in Table S5†) and catalyst concentration (as seen in Table S8†) within it, we found that its k'_t value increased rapidly with altitude as the concentration of FA decreases by ~6 times and k_t value increases by 3 orders of magnitude with increasing altitude from 5 km to 15 km. Besides, compared with the value of k_R, we found that the rate ratio of k'_t(RFA1_s)/k_R increased from 0.03% at 0 km to 24.2% at 15 km. This implies that, as we move towards higher altitude, the contribution of HCOOH to the HO_2 + Cl → HCl + O_2 reaction cannot be neglected at high altitude.

4. Summary and conclusions

In this work, the hydrogen abstraction of the HO_2 + Cl → HCl + $^3O_2$ reaction catalyzed by H_2O, NH_3 and HCOOH has been investigated theoretically using the CCSD(T)-F12A/VDZ-F12//M06-2X/6-311++G(2d,2p) method and canonical vibrational transition (CVT) state theory with the small curvature tunneling (SCT) correction. The conclusions obtained in this investigation are summarized as follows:

As for the three catalytic reactions, there are two entry channels: namely a stepwise route and a one elementary step, and this article has discovered that the stepwise route is more favorable than the corresponding one elementary step. Meanwhile, for the stepwise route, single and double hydrogen atom transfer pathways are involved, and the calculation results indicate that the former pathway has more advantages than the latter in all three catalytic reactions.

For the stepwise process of X···HO_2 (X = H_2O, NH_3 and HCOOH) + Cl reaction, at 0 km altitude, none of the HO_2 + Cl → HCl + O_2 reactions with catalysts of H_2O, NH_3, and HCOOH can compete with the reaction without a catalyst, as all the rate ratios between reaction with a catalyst and without a catalyst are less than 0.6% within the temperature range 280–320 K. In addition, at higher altitudes in the troposphere, it was shown that at altitudes of 5, 10 and 15 km, the catalytic effect of HCOOH for the gas-phase oxidation reaction of HO_2 by Cl is larger than those of H_2O or NH_3. Furthermore, the rate ratio of k'_t(RFA1_s)/k_R increases from 0.03% at 0 km to 24.2% at 15 km. This implies that the contribution of HCOOH to the HO_2 + Cl → HCl + O_2 reaction cannot be neglected at high altitudes. This present study presents a new mechanism for understanding the gas-phase oxidation reaction of HO_2 by Cl *via* H_2O, NH_3 and HCOOH catalysis. Moreover, the new mechanisms have wide applications in investigating gas-phase hydrogen abstraction. Therefore, the present results could also be of great importance for elucidating and understanding other atmospheric oxidation processes with neutral, basic, and acidic catalysts.

Conflicts of interest

There are no conflicts to declare.

Acknowledgements

This work was supported by the National Natural Science Foundation of China (No. 21603132, 21473108), the Funds of Research Programs of Shaanxi University of Technology (No. SLGQD13(2)-3, SLGQD13(2)-4), the Shanghai Science and Technology Committee (16DZ2270100), and the Shaanxi Provincial Natural Science Foundation (No. 2019JM-336).

References

1 Y. Tang, G. S. Tyndall and J. J. Orlando, *J. Phys. Chem. A*, 2010, **114**, 369–378.
2 P. D. Lightfoot, R. A. Cox, J. N. Crowley, M. Destriau, G. D. Hayman, M. E. Jenkin, G. K. Moortgat and F. Zabel, *Atmos. Environ.*, 1992, **26**, 1805–1961.
3 D. Stone, L. K. Whalley and D. E. Heard, *Chem. Soc. Rev.*, 2012, **41**, 6348–6404.
4 S. S. Prasad, R. L. Jaffe, R. C. Whitten and R. P. Turco, *Planet. Space Sci.*, 1978, **26**, 1017–1026.
5 S. C. Wofsy, *Eos, Transactions American Geophysical Union*, 1999, **80**, 468.
6 W. C. Keene, J. Stutz, A. A. P. Pszenny, J. R. Maben, E. V. Fischer, A. M. Smith, R. V. Glasow, S. Pechtl, B. C. Sive and R. K. Varner, *J. Geophys. Res.: Atmos.*, 2007, **112**, D10S12.
7 C. W. Spicer, E. G. Chapman, B. J. Finlaysonpitts, R. A. Plastridge, J. M. Hubbe, J. D. Fast and C. M. Berkowitz, *Nature*, 1998, **394**, 353–356.
8 O. Dobis and S. W. Benson, *J. Am. Chem. Soc.*, 1993, **115**, 8798–8809.
9 K. M. Hickson and L. F. Keyser, *J. Phys. Chem. A*, 2005, **109**, 6887–6900.
10 R. Riffault, Y. Bedjanian and G. L. Bras, *Int. J. Chem. Kinet.*, 2001, **33**, 317–327.

11 M. Weissman, L. G. S. Shum, S. P. Heneghan and S. W. Benson, *J. Phys. Chem.*, 1981, **85**, 2863–2866.
12 R. Atkinson, D. Baulch, R. Cox, J. Crowley, R. Hampson Jr, J. Kerr, M. Rossi and J. Troe, *IUPAC Subcommittee on gas kinetic data evaluation for atmospheric chemistry*, 2001, vol. 20.
13 J. Burrows, D. Cliff, G. W. Harris, B. A. Thrush and J. Wilkinson, *Proc. R. Soc. London, Ser. A*, 1979, **368**, 463–481.
14 F. C. Cattell and R. A. Cox, *J. Chem. Soc., Faraday Trans. 2*, 1986, **82**, 1413–1426.
15 R. A. Cox, *Int. J. Chem. Kinet.*, 1980, **12**, 649–660.
16 Y. P. Lee and C. J. Howard, *J. Chem. Phys.*, 1982, **77**, 756–763.
17 R. J. Buszek, J. S. Francisco and J. M. Anglada, *Int. Rev. Phys. Chem.*, 2011, **30**, 335–369.
18 R. J. Buszek, M. Torrent-Sucarrat, J. M. Anglada and J. S. Francisco, *J. Phys. Chem. A*, 2012, **116**, 5821–5829.
19 N. Butkovskaya, M. T. Rayez, J. C. Rayez, A. Kukui and G. L. Bras, *J. Phys. Chem. A*, 2009, **113**, 11327–11342.
20 N. Kanno, K. Tonokura, A. Tezaki and M. Koshi, *J. Phys. Chem. A*, 2005, **109**, 3153–3158.
21 K. Suma, Y. Sumiyoshi and Y. Endo, *Science*, 2006, **311**, 1278–1281.
22 T. Zhang, W. Wang, P. Zhang, J. Lü and Y. Zhang, *Phys. Chem. Chem. Phys.*, 2011, **13**, 20794–20805.
23 J. C. Hansen and J. S. Francisco, *ChemPhysChem*, 2002, **3**, 833–840.
24 V. Vaida, H. G. Kjaergaard, P. E. Hintze and D. J. Donaldson, *Science*, 2003, **299**, 1566–1568.
25 J. Zuo, Y. Li, H. Guo and D. Xie, *J. Phys. Chem. A*, 2016, **120**, 3433–3440.
26 S. Mallick and P. Kumar, *J. Phys. Chem. A*, 2018, **122**, 7151–7159.
27 G. H. Mount, B. Rumburg, J. Havig, B. Lamb, H. Westberg, D. Yonge, K. Johnson and R. Kincaid, *Atmos. Environ.*, 2002, **36**, 1799–1810.
28 S. M. Wilson and M. L. Serre, *Atmos. Environ.*, 2007, **41**, 4977–4987.
29 B. Bandyopadhyay, P. Biswas and P. Kumar, *Phys. Chem. Chem. Phys.*, 2016, **18**, 15995–16004.
30 B. Bandyopadhyay, P. Kumar and P. Biswas, *J. Phys. Chem. A*, 2017, **121**, 3101–3108.
31 R. J. Buszek, A. Sinha and J. S. Francisco, *J. Am. Chem. Soc.*, 2011, **133**, 2013–2015.
32 S. G. Da, *Angew. Chem., Int. Ed.*, 2010, **49**, 7523–7525.
33 S. Ghoshal and M. K. Hazra, *RSC Adv.*, 2015, **5**, 17623–17635.
34 M. K. Hazra and T. Chakraborty, *J. Phys. Chem. A*, 2005, **109**, 7621–7625.
35 M. K. Hazra and T. Chakraborty, *J. Phys. Chem. A*, 2006, **110**, 9130–9136.
36 D. Josa, J. Rodríguez-Otero, E. M. Cabaleiro-Lago and M. Rellán-Piñeiro, *Chem. Phys. Lett.*, 2013, **557**, 170–175.
37 M. Walker, A. J. Harvey, A. Sen and C. E. Dessent, *J. Phys. Chem. A*, 2013, **117**, 12590–12600.
38 N. Bork, L. Du, H. Reiman, T. Kurtén and H. G. Kjaergaard, *J. Phys. Chem. A*, 2014, **118**, 5316–5322.
39 Y. Zhao and D. G. Truhlar, *Theor. Chem. Acc.*, 2008, **119**, 525.
40 J. Elm, M. Bilde and K. V. Mikkelsen, *J. Chem. Theory Comput.*, 2012, **8**, 2071–2077.
41 F. Y. Liu, X. F. Tan, Z. W. Long, B. Long and W. J. Zhang, *RSC Adv.*, 2015, **5**, 32941–32949.
42 B. Long, X. F. Tan, C. R. Chang, W. X. Zhao, Z. W. Long, D. S. Ren and W. J. Zhang, *J. Phys. Chem. A*, 2013, **117**, 5106–5116.
43 K. Fukui, *Acc. Chem. Res.*, 1981, **14**, 363–368.
44 C. Gonzalez and H. B. Schlegel, *J. Chem. Phys.*, 1989, **90**, 2154–2161.
45 M. Page and J. W. McIver Jr, *J. Chem. Phys.*, 1988, **88**, 922–935.
46 M. J. Frisch, G. Trucks and J. A. Pople, *et al.*, *Gaussian 09, Revision A.01*, Gaussian Inc, Pittsburgh, PA, 2009.
47 N. Bork, J. Elm, T. Olenius and H. Vehkamäki, *Atmos. Chem. Phys.*, 2014, **14**, 12023–12030.
48 J. Elm and K. Kristensen, *Phys. Chem. Chem. Phys.*, 2017, **19**, 1122–1133.
49 N. Myllys, J. Elm, R. Halonen, T. Kurtén and H. Vehkamäki, *J. Phys. Chem. A*, 2016, **120**, 621–630.
50 F. Neese, *Wiley Interdiscip. Rev.: Comput. Mol. Sci.*, 2012, **2**, 73–78.
51 B. Long, J. L. Bao and D. G. Truhlar, *Proc. Natl. Acad. Sci. U. S. A.*, 2018, **115**, 6135–6140.
52 B. Long, J. L. Bao and D. G. Truhlar, *J. Am. Chem. Soc.*, 2018, **141**, 611–617.
53 B. Long, J. L. Bao and D. G. Truhlar, *Nat. Commun.*, 2019, **10**, 2003.
54 B. C. Garrett, D. G. Truhlar, R. S. Grev and A. W. Magnuson, *J. Phys. Chem.*, 1980, **84**, 1730–1748.
55 Y. P. Liu, G. C. Lynch, T. N. Truong, D. H. Lu, D. G. Truhlar and B. C. Garrett, *J. Am. Chem. Soc.*, 1993, **115**, 2408–2415.
56 Y. Chuang, J. Corchado, P. Fast, J. Villa, E. Coitino, W. Hu, Y. Liu, G. Lynch, K. Nguyen and C. Jackels, *Polyrate-version 8.2*, University of Minnesota, Minneapolis [CP], 1999.
57 D. L. Singleton and R. J. Cvetanovic, *J. Am. Chem. Soc.*, 1976, **98**, 6812–6819.
58 J. L. Bao, P. Seal and D. G. Truhlar, *Phys. Chem. Chem. Phys.*, 2015, **17**, 15928–15935.
59 M. L. Wei, X. F. Tan, Z. W. Long and B. Long, *RSC Adv.*, 2017, **7**, 56211–56219.
60 X. Chen, Y. F. Zhao, L. S. Wang and J. Li, *Comput. Theor. Chem.*, 2017, **1107**, 57–65.
61 Y. Zhao, X. Chen and J. Li, *Nano Res.*, 2017, **10**, 3407–3420.
62 X. Chen, C. Tao, L. Zhong, Y. Gao, W. Yao and S. Li, *Chem. Phys. Lett.*, 2014, **608**, 272–276.
63 B. Long, X. Tan, Z. Long, Y. Wang, D. Ren and W. Zhang, *J. Phys. Chem. A*, 2011, **115**, 6559–6567.
64 T. Zhang, R. Wang, H. Chen, S. Min, Z. Wang, C. Zhao, Q. Xu, L. Jin, W. Wang and Z. Wang, *Phys. Chem. Chem. Phys.*, 2015, **17**, 15046–15055.
65 T. Zhang, R. Wang, W. Wang, S. Min, Q. Xu, Z. Wang, C. Zhao and Z. Wang, *Comput. Theor. Chem.*, 2014, **1045**, 135–144.
66 T. Zhang, C. Yang, X. Feng, J. Kang, L. Song, Y. Lu, Z. Wang, Q. Xu, W. Wang and Z. Wang, *Phys. Chem. Chem. Phys.*, 2016, **18**, 17414–17427.

67 J. Gonzalez, M. Torrent-Sucarrat and J. M. Anglada, *Phys. Chem. Chem. Phys.*, 2010, **12**, 2116–2125.
68 C. T. Chang, T. H. Liu and F. T. Jeng, *Environ. Res.*, 2004, **94**, 67–74.
69 J. M. Anglada, R. Crehuet and A. Solé, *Mol. Phys.*, 2019, 1–12.
70 H. A. Rypkema, A. Sinha and J. S. Francisco, *J. Phys. Chem. A*, 2015, **119**, 4581–4588.
71 M. K. Hazra and S. Amitabha, *J. Am. Chem. Soc.*, 2011, **133**, 17444–17453.
72 B. Long, Z. Long, Y. Wang, X. Tan, Y. Han, C. Long, S. Qin and W. Zhang, *ChemPhysChem*, 2012, **13**, 323–329.
73 B. Long, J. L. Bao and D. G. Truhlar, *J. Am. Chem. Soc.*, 2016, **138**, 14409–14422.
74 T. Zhang, X. Lan, Z. Qiao, R. Wang, X. Yu, Q. Xu, Z. Wang, L. Jin and Z. Wang, *Phys. Chem. Chem. Phys.*, 2018, **20**, 8152–8165.
75 T. Zhang, W. Wang, C. Li, Y. Du and J. Lü, *RSC Adv.*, 2013, **3**, 7381–7391.
76 S. Sarkar, S. Mallick, D. Kaushik, P. Kumar and B. Bandyopadhyay, *Phys. Chem. Chem. Phys.*, 2017, **19**, 27848–27858.
77 V. P. Aneja, D. R. Nelson, P. A. Roelle, J. T. Walker and W. Battye, *J. Geophys. Res.: Atmos.*, 2003, **108**, 2156–2202.
78 G. Brasseur, J. J. Orlando and G. S. Tyndall, *Atmospheric chemistry and global change*, Oxford University Press, 1999.
79 J. X. Warner, Z. Wei, L. L. Strow, R. Dickerson and J. Nowak, *Atmos. Chem. Phys. Discuss.*, 2015, **15**, 35823–35856.
80 N. Hiranuma, S. D. Brooks, D. C. Thornton and B. W. Auvermann, *J. Air Waste Manag. Assoc.*, 2010, **60**, 210–218.
81 A. Razavi, F. Karagulian, L. Clarisse, D. Hurtmans, P. F. Coheur, C. Clerbaux, J. F. Müller and T. Stavrakou, *Atmos. Chem. Phys.*, 2010, **10**, 857–872.
82 M. W. Shephard, A. Goldman, S. A. Clough and E. J. Mlawer, *J. Quant. Spectrosc. Radiat. Transf.*, 2003, **82**, 383–390.
83 J. M. Anglada, G. J. Hoffman, L. V. Slipchenko, M. M. Costa, M. F. Ruiz-Lopez and J. S. Francisco, *J. Phys. Chem. A*, 2013, **117**, 10381–10396.
84 S. Mallick, S. Sarkar, B. Bandyopadhyay and P. Kumar, *J. Phys. Chem. A*, 2017, **122**, 350–363.